

ASE: Practical Acoustic Speed Estimation Beyond Doppler via Sound Diffusion Field

Sheng Lyu

shenglyu@connect.hku.hk
The University of Hong Kong
Hong Kong, China

Chenshu Wu

chenshu@cs.hku.hk
The University of Hong Kong
Hong Kong, China

ABSTRACT

Passive human speed estimation plays a critical role in acoustic sensing. Despite extensive study, existing systems, however, suffer from various limitations: First, the channel measurement rate proves inadequate to estimate high moving speeds. Second, previous acoustic speed estimation exploits Doppler Frequency Shifts (DFS) created by moving targets and relies on microphone arrays, making them only capable of sensing the radial speed within a constrained distance. To overcome these issues, we present ASE, an accurate and robust Acoustic Speed Estimation system on a single commodity microphone. We propose a novel Orthogonal Time-Delayed Multiplexing (OTDM) scheme for acoustic channel estimation at a high rate that was previously infeasible, making it possible to estimate high speeds. We then model the sound propagation from a unique perspective of the acoustic diffusion field, and infer the speed from the acoustic spatial distribution, a completely different way of thinking about speed estimation beyond prior DFS-based approaches. We further develop novel techniques for motion detection and signal enhancement to deliver a robust and practical system. We implement and evaluate ASE through extensive real-world experiments. Our results show that ASE reliably tracks walking speed, independently of target location and direction, with a mean error of 0.13 m/s, a reduction of 2.5x from DFS, and a detection rate of 97.4% for large coverage, *e.g.*, free walking in a $4\text{m} \times 4\text{m}$ room. We believe ASE pushes acoustic speed estimation beyond the conventional DFS-based paradigm and inspires exciting research in acoustic sensing.

1 INTRODUCTION

Capturing the portraits of indoor human activities is an enduring task in the wide sensing community [34, 49, 73, 79, 88]. Frequently, human subjects are in motion, rendering passive speed estimation one of the most fundamental components in human sensing. At the heart of understanding the physical state of moving subjects, speed provides valuable insights into human behaviors and health. With speed profiles, a broad range of applications can be accommodated, such as gait recognition [17, 74, 80], fall detection [27, 37], human

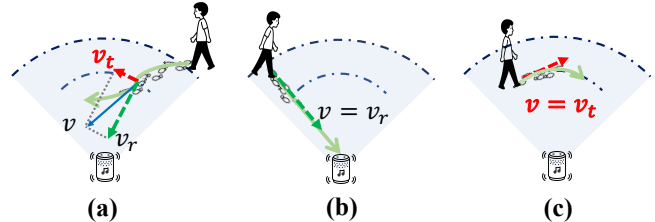


Figure 1: ASE vs. DFS. Walking speed \vec{v} can be decomposed to radial speed v_r and tangent speed v_t . DFS can only capture radial speed v_r , but fails to capture v_t . Conversely, ASE can capture both v_r and v_t , a complete estimation of v .

activity recognition [23, 45, 90], tracking [14, 41, 49], gesture control [70], fitness tracking [61, 74, 81], *etc.*

Particularly, walking speed estimation plays an important role in wellbeing monitoring. It is increasingly perceived as the sixth vital sign [20, 42] which is closely associated with and predictive of one’s health conditions [74]. Slowing walking speed suggests increased frailty, leading to potential physical and cognitive decline [52, 53]. Moreover, walking speed acts as a biomarker for gait recognition [75] and an effective indicator of risky falls [27]. Enabling these applications calls for accurate and robust speed estimation, preferably in a contactless and passive manner.

Passive speed estimation, however, is a long-standing open challenge. Various approaches have been proposed for indoor speed estimation using vision systems [7, 10], wireless signals [71, 74, 86], and acoustic signals [14, 38, 83]. Camera-based approaches, such as VICON motion capture system [10], usually provide the most accurate speed but require complex and expensive hardware setups and are limited within a functional area. Wireless sensing has recently been extensively studied, yet mostly relies on specialized radars [3, 6, 72, 77], or certain WiFi chipsets [5, 8, 25].

Acoustic devices, such as smart speakers [1, 2], are now widely and interactively available in our everyday lives, often as plug-and-play devices with co-located microphones and speakers, making acoustic sensing an increasingly hot topic in recent years [18, 19, 56, 63, 64, 88]. The widespread usage of such audio devices hold substantial potential for enabling

significant applications, provided that accurate and robust speed estimation can be achieved through acoustic sensing.

Existing acoustic speed estimation mostly relies on the Doppler Frequency Shifts (DFS) caused by target movements to derive the speed [37, 84]. These approaches, however, suffer from three major limitations in acoustic speed estimation:

- The low sound speed imposes an innate limit on the maximum Channel State Information (CSI) rate achievable on an acoustic channel [88], which unfortunately is insufficient for estimating high speeds (e.g., typical walking speed of around 1 m/s).
- Depending on the specific moving direction and location, Doppler-based approaches can only capture the partial speed projected in a radial direction that creates reflection path length changes and thus frequency shifts [49, 69], as shown in Fig. 1.
- DFS often only utilizes one or a few reflection paths off the target for sensing, leading to performance degradation with the increase of distance, e.g., over 1 m [33, 34, 38, 70, 88], and thereby confining them for short-range sensing.

To overcome these limitations, we pose a crucial research question: *Can we achieve robust and location-independent acoustic speed estimation beyond DFS-based approaches?* In this work, we present *ASE*, a complete novel pipeline that achieves practical acoustic speed estimation using only a *single* microphone channel. At a high level, it includes 1) a brand new modulation scheme that breaks the upper limit of acoustic CSI, 2) a novel theoretical model that can derive the whole speed rather than solely radial speed, and 3) a set of innovative techniques that make *ASE* more robust.

Regarding the first challenge, we propose a novel Orthogonal Time Delayed Multiplexing (OTDM) scheme. Detailed analysis reveals that the CSI rate is inherently limited by the travel speed of sound and the propagation distance. This limitation restricts acoustic devices from estimating high speeds, presenting a fundamental challenge in acoustic speed estimation. Inspired by OFDM, we develop a specialized modulation framework to mix the signals effectively without extra cost. Technically, we leverage the separation ability of orthogonal signals to send two signals concurrently, while delaying one sequence for half of the frame time. Through this approach, we can effectively atomize the original frame to its half and boost 2x of the CSI rate.

To surpass Doppler-based speed estimation, we build a comprehensive model that can capture the entire speed. Our model builds upon the acoustic diffusion model, as illustrated in Fig. 3. Specifically, we investigate the fundamental properties of sound diffusion indoors and introduce a concise approach for speed estimation. We draw aspiration from previous physical studies of room acoustics [31], which model the diffusive sound propagation. Conceptually, *ASE* employs the distinct spatial distribution of sound pressure field. The

analysis of spatial-temporal properties of the sound field shows that the correlation of the sound energy embodies the speed of a moving target. Although Autocorrelation Function (ACF) has been employed for extracting periodic vital signs [24, 66], building the bridge between ACF of sound and speed is new and non-trivial. In *ASE*, we establish the relationship in the context of the acoustic diffusion field and model the ACF of acoustic CSI as a function of the moving speed. Different from DFS, the proposed model statistically leverages all the reflection signals, and integrates over all possible directions, thus making speed estimation less dependent on the moving location and direction and building a novel foundation for speed estimation with commodity acoustic devices.

We also incorporate several effective designs to transform *ASE* into a practical system. We employ pseudo-noise code in *ASE* with nice orthogonality and tolerance to interference, for CSI estimation from inaudible sound signals. By careful modulation and filtering, the sensing signals are made hardly audible compared to previous designs like the widely used chirps [64], which are considerably intrusive to human ears in practice. Moreover, we identify robust motion indicators and devise an effective approach that embraces frequency diversity to significantly boost the weak signals for speed estimation, which largely extends the sensing coverage and improves the speed estimation accuracy.

We prototype *ASE* on commodity audio devices. We conduct comprehensive experiments to evaluate *ASE* for diverse walking behaviors in real-world indoor scenarios. The results show that *ASE* achieves a mean speed accuracy of 0.13 m/s with a 90%-tile error of < 0.2 m/s and an overall detection rate of 97.4% in a $4\text{m} \times 4\text{m}$ room, significantly outperforming prior DFS-based approach, which yields a 2.5 \times higher mean error under the same conditions. We further conduct case studies on human activity recognition, fall detection, and gait analysis as potential applications by profiling the speeds of different human activities. The superior performance validates *ASE* and its underlying model as a new paradigm of acoustic speed estimation for many applications.

Contributions: We believe *ASE* lays a completely new foundation for acoustic speed estimation and offers new insights into the field by making the following core contributions:

- We develop OTDM, the first-of-its-kind modulation scheme that allows acoustic CSI estimation at a high rate exceeding the previous maximum possible rate.
- To the best of our knowledge, we are the first to employ the sound diffusion model for speed estimation and integrate it with the acoustic channel. The model fundamentally differs from DFS-based approaches.
- We design and implement *ASE* system using a single commodity microphone. We incorporate a pipeline of distinct

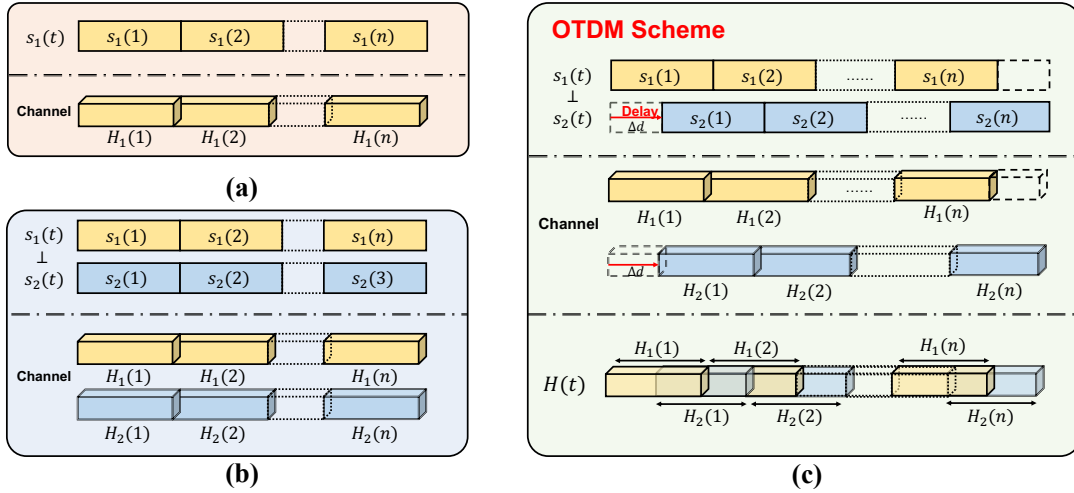


Figure 2: OTDM Scheme. (a) Given $s_1(t)$, the channel is estimated by frame. (b) Given orthogonal sequences $s_1(t)$ and $s_2(t)$, we can get two channel estimations at the same time. (c) Orthogonal sequences $s_1(t)$ and $s_2(t)$, with $s_2(t)$ delayed by Δd , are modulated into one sequence $s(t)$. $H_1(t)$ and $H_2(t)$ estimated from the two sequences are concatenated into $H(t)$ alternately.

techniques and conduct experiments to validate its superior performance to prior approaches.

2 OTDM DESIGN

We first discuss the contradiction between high speed estimation and acoustic CSI rate. After that, we will present our novel solution of Orthogonal Time Delayed Multiplexing (OTDM) scheme to boost the CSI rate.

2.1 High Speed & Low CSI Rate Dilemma

Initially, we will discuss a universal problem of acoustic speed estimation. To profile speed information, a common practice is to estimate Channel State Information (CSI), which characterizes how sound propagates in a Tx/Rx system. The CSI rate F_s refers to how many CSIs we can acquire per second in the system. However, the inadequacy of acoustic CSI rate imposes a fundamental challenge for speed estimation. Conceptually, the lower CSI sampling rates we acquire, the smaller the maximum frequency shift can be observed. Given a CSI rate of F_s , the maximum frequency shift detectable on the Doppler spectrum is $F_s/2$. Assuming a carrier frequency of f , the maximum measurable speed is

$$v_{\max} = \frac{F_s}{2 \cdot f} \cdot c, \quad (1)$$

which is only 0.4 m/s considering $f = 20$ kHz and $F_s = 49$ Hz. When factoring in noise, this obviously falls short of measuring typical indoor walking speeds.

Then another question arises: can we increase the acoustic CSI rate? Unfortunately, slow sound speed imposes an inherent limitation on the maximum achievable CSI rate on an acoustic channel. Assuming the sampling rate of acoustic

signal is f_s (note that f_s is very different from the CSI rate F_s), plus x -m propagation path, then the CSI rate is given by

$$F_s = \frac{f_s}{x/c \cdot f_s} = \frac{c}{x}. \quad (2)$$

As we can see, if we want to increase the CSI rate, the only way is to limit the sensing distance. For example, considering the in-air sound speed of 343 m/s and the longest propagation path of 7 meters, the minimum channel measurement interval should be larger than 20 ms, resulting in a CSI rate of 50 Hz. However, even if we narrow this range to 3.5 meters, the maximum possible CSI rate without causing signal mixture only increases to 100 Hz, still insufficient for estimating human walk speed around 1 m/s.

This observation reminds us that current CSI rate cannot support high speed estimation for daily activities (e.g., walking), and it is infeasible to increase CSI rate given the sensing distance for current channel design. To tackle this problem, we present a novel OTDM design in the next section.

2.2 OTDM Transmission Scheme

Based on the above discussion, we find a challenging contradiction for acoustic speed estimation: Given the current channel design, it is impracticable to enhance the CSI rate, while not reducing the sensing range or causing signal mixture. The underlying core of this dilemma is we have not fully utilized the channel capacity. If we can estimate the channel simultaneously while having some temporal delay, can we split the channel in more atomized frame clips, hereby increasing the CSI rate? Motivated by this idea, we are inspired to design a novel modulation scheme that leverages the separability of orthogonal signals. The key idea is, by using

orthogonal signals, we can transmit multiple sensing signals concurrently over the same physical channel (*i.e.*, speaker-microphone pair) and perform channel estimation separately, which brings more samples of the channel measurements. If we further shift the multiple orthogonal signals by a certain amount of time, we effectively obtain finer-grained CSI measurements in the time domain, *i.e.*, a higher CSI rate. We name it Orthogonal Time-Delayed Multiplexing (OTDM) transmission. By OTDM, the duration and interval of each separate sensing signal will not be shortened.

Suppose we have two sequences $s_1(t)$ and $s_2(t)$ with decent orthogonality over time. Then we can transmit them concurrently, while still being able to separate them on the receiver side by using correlation. Previous orthogonal transmission schemes typically transmit synchronized signals. Differently, as shown in Fig. 2, to enhance the CSI rate, we need to delay one sequence by $\Delta d = N_s/2$, where N_s is the default sensing interval as described in §4.1. Then we can acquire two sets of channel estimation: $H_1 \in \mathbb{R}^n$ and $H_2 \in \mathbb{R}^n$. Then the two CSI measurements, estimated from the two orthogonal sequences respectively, characterize the physical channel independently, yet at a slightly shifted time. Therefore, by stacking the two series of CSI measurements, *i.e.*, $[H_1(1), H_2(1), \dots, H_1(n), H_2(n)]$, we can double the CSI rate from $1/N_s$ to $2/N_s$ without shortening the sequence length (*i.e.*, signal duration). Our extensive experiment will show the effectiveness of OTDM design. We will detail the design for the most common case (*i.e.*, one speaker) in §4.2, while our scheme can generalize to more.

3 ACOUSTIC DIFFUSION SPEED MODEL

Conventional approaches for speed estimation relying on DFS can only measure the radial speed, making it a location- and direction-dependent solution, as shown in Fig. 1. In this section, we will introduce a novel theoretical model for capturing the complete speed. Our model is primarily inspired by room acoustics [31]. In below, we first briefly review statistical room acoustics and then establish the model that works with channel measurements on commodity audio devices.

3.1 Limitations of DFS

Existing DFS-based acoustic speed estimation implicitly or explicitly relies on a simplistic propagation model. These methods typically involve identifying the primary reflection path between the human body and audio devices and deducing the DFS from the corresponding bins. Consequently, these techniques yield only partial information regarding speed estimation [44, 86], specifically the radial speed v_r between the human and acoustic device pair, neglecting the tangent component v_t , as illustrated in Fig. 1. Essentially, if we only consider one or a few reflection paths, the tangent component will be inevitably lost. Fortunately, we notice

that the acoustic signals will be scattered by the numerous reflectors to different directions in the environment, as can be seen from Fig. 3(b) and Fig. 4. If we can efficiently leverage the multi-path reflections, it equivalently creates various estimations of speed along different directions. Conceptually, the reflectors can be regarded as many "virtual speakers", offering numerous speed observations of different tangent components. From a statistical perspective, we can imagine these speed components are synthesized into a complete estimation of speed v , which contains both radial speed v_r and tangent speed v_t . To this end, we explore the propagation properties of sound and derive the speed information from a statistical approach. We will first introduce acoustic diffusion model in §3.2 and generalize it to CSI in §3.3.

3.2 Sound Diffusion Field

Given a bounded sound propagation scenario (*e.g.*, indoor space), the sound energy is partly reflected/scattered by the obstacles, as shown in Fig. 3. Considering a moving target in space that continuously distorts the sound propagation, a diffuse sound field will be created due to the continuous redistribution of sound energy, especially in an environment with rich diffuseness such as a room. Thus according to the acoustic wave equation [47], we can express the sound pressure as $p = p(x, t) = Ae^{j(\omega t - \vec{k} \cdot \vec{r})}$, where A denotes the amplitude, ω is the frequency of the wave, \vec{k} indicates the propagation vector, and c is the propagation speed of sound. r is the position vector, *i.e.*, $\vec{r} = x\vec{i} + y\vec{j} + z\vec{k}$. Assume the space is excited by a limited-band signal, and consider two adjacent observation points a and b separated by a distance of x , as shown in Fig. 3. The sound pressure is expressed as $p_a(t) = A \cos(\omega t - \phi)$ and $p_b(t) = A \cos(\omega t - \phi - kx \cos(\theta))$, respectively, where θ denotes the direction of the incident sound wave, A and ϕ are random amplitudes and angles, and k and ω represent the wave number and center frequency of the sound signals. The correlation coefficient of the sound energy over space provides insight into the degree of diffuseness. Specifically, the spatial correlation over $p_a(t)$ and $p_b(t)$ is expressed as

$$\psi_p = \frac{\overline{p_a(t)p_b(t)}}{\sqrt{\overline{p_a(t)^2} \cdot \overline{p_b(t)^2}}}, \quad (3)$$

where ψ_p represents the correlation coefficient, and $\overline{\cdot}$ denotes operation of time average. Since sound is a plane wave, we can derive the time average of $p_a(t)^2$ and $p_b(t)^2$ both as $\frac{A^2}{2}$, and meanwhile, the average of the product of sound pressure is computed as $\overline{p_a(t)p_b(t)} = \frac{1}{\Delta t} \int_t^{t+\Delta t} p_a(t)p_b(t)dt = \frac{A^2}{2} \cos(kx \cos \theta)$. Therefore, by substituting them into Eq. (3), we derive the correlation for the direction of incidence θ as

$$\psi_p(x, \theta) = \cos(kx \cos \theta). \quad (4)$$

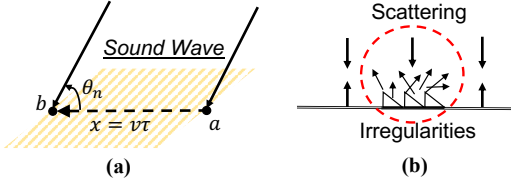


Figure 3: Sound Diffusion Model. (a) The sound wave traverses while an object is moving $a \rightarrow b$. (b) The sound wave is diffusive in all directions by irregular reflectors.

Then by integrating Eq. (4) over all directions, we can obtain the spatial correlation of the total sound pressure. If we consider the the incident sound waves are distributed in a plane, namely 2D model, we can get

$$\psi_p(x) = \frac{1}{2\pi} \int_0^{2\pi} \psi(x, \theta) d\theta = J_0(kx), \quad (5)$$

where $J_0(x) = \frac{1}{2\pi} \int_0^{2\pi} \cos(x \cos \theta) d\theta$ is the 0th-order Bessel function of its first kind. If we consider 3D scattering model, *i.e.*, the sound waves are distributed in a sphere, we can acquire the correlation coefficient as,

$$\psi_p(x) = \frac{1}{4\pi} \int_0^\pi \int_0^{2\pi} \psi(x, \theta) d\phi d\theta = \frac{\sin(kx)}{kx}, \quad (6)$$

where ϕ is the azimuth angle, varying from 0 to 2π . Further considering a target moving from point a to b at a speed of v , we have $x = v\tau$, where τ is the traveling time. Thus, the above equation can be written as

$$\psi_p(v; \tau) = \frac{\sin(kv\tau)}{kv\tau}. \quad (7)$$

It bridges the spatial correlation of the sound pressure ψ_p with a target's moving speed v , independent of the moving direction and location. Note that in both scenarios, we average diffuseness across *all directions*, which differs from DFS that only takes the radial speed into consideration, promising a potential approach for speed estimation beyond the Doppler-based approach. To achieve ASE, however, we need to investigate how to obtain ψ_p on commodity audio devices.

3.3 Acoustic Speed Estimation

In this section, we investigate CSI measured on commodity audio devices and extend Eq. (7) to the ACF of acoustic CSI. **Channel Power:** Indoor space proves to be an environment with rich diffuseness [31], where the above acoustic diffusion model applies. However, it is infeasible to directly measure the sound pressure without professional equipments. It is crucial to efficiently estimate sound pressure on common devices. In ASE, we approximate the sound pressure as the power of the sound diffusion field. Sound pressure can be considered as the equivalent of the power of CSI [32]. CSI is the linear aggregation of multi-path components, which

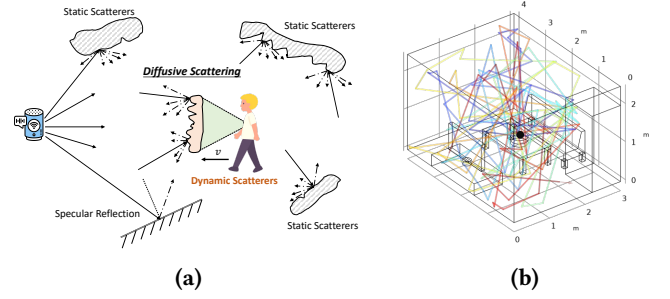


Figure 4: Diffusive Scattering in the room. (a) Illustration of diffusion scattering and specular reflections. The acoustic waves not only experiences specular reflections, but also diffusive scatterings on any non-flat planes. (b) A simulation result of how acoustic wave is reflected and scattered in a common room. The black point emits the acoustic rays with frequency range 17k-20kHz. By employing the rich multi-path semantics, these scatterers are creating "virtual speakers", thus creating different views of speed estimation.

can then be decomposed into two parts, *i.e.*, the static part Λ_S attributed to static scatterers and the dynamic part Λ_D contributed by dynamic scatterers, typically from human subjects, as shown in Fig. 4. To sum up, we can model the relationship between channel power and sound pressure as

$$G(f, t) = |H(f, t)|^2 + \epsilon(f, t) \approx |p(f, t)|^2 + n(f, t) = \left| \sum_{i \in \Lambda_D} p_i(f, t) + \sum_{i \in \Lambda_S} p_i(f, t) \right|^2 + n(f, t), \quad (8)$$

where $H(f, t)$ represents CSI at time t and subcarrier f . Practically, the static components are cancelled by removing the time average from $H(f, t)$. $\epsilon(f, t)$ and $n(f, t)$ are noise terms, with a variance of $\Sigma_N(f)$. $p(f, t)$ is the sound pressure, which is further decomposed as the dynamic and static components. $p_i(f, t)$ is the sound pressure contributed by the i^{th} scatterer, which can also be deemed as mutually independent of $p_j(f, t)$, $\forall i \neq j$, in sound diffusion field. Next, we model the spatial properties of $G(f, t)$ for speed estimation. **Speed Estimation Model:** To learn the spatial distribution of channel power $G(f, t)$, we compute the ACF function, *i.e.*,

$$\psi_G(f, t, \tau) = \frac{\mathbb{E} [G(f, t)G^H(f, t + \tau)]}{\mathbb{E} [G(f, t)G^H(f, t)]} \triangleq \frac{\mathcal{R}_1}{\mathcal{R}_2}. \quad (9)$$

Given that $p_i(f, t)$ for any $i \in \Lambda_D$ and $p_j(f, t)$ for any $j \in \Lambda_S$ are mutually independent, and considering that sound pressures induced by static scatterers are statistically characterized by a zero mean, *i.e.*, $\mathbb{E}[p_j(f, t)] = 0, \forall j \in \Lambda_S$, it follows that any term involving a static component from Λ_S in a product will be canceled in expectation. Specifically, $\forall i \in \Lambda_D$ and $\forall j \in \Lambda_S$, we have $\mathbb{E}[p_i(f, t)p_j(f, t)] = 0$. Let

$P_D(t) = \sum_{i \in \Lambda_D} p_i(f, t)$, we have

$$\begin{aligned} \mathcal{R}_1 &\approx \mathbb{E} [P_D(t)P_D^H(t+\tau)] + \mathbb{E} [N(t)N^H(t+\tau)] \\ &= \Theta_D^H \cdot \Psi_D + \Sigma_N(f) \cdot \mathbf{I}_n, \end{aligned} \quad (10)$$

where $N(t) = [n(f_1, t), n(f_2, t), \dots, n(f_{N_f}, t)]$, N_f is the number of subcarriers. $\mathbf{I}_n \in \mathbf{R}^{N_\tau}$ is identity matrix, N_τ is the number of time lag for ACF. $\Psi_D \in \mathbf{R}^{N_\tau \times N_D}$ is the ACF matrix of sound pressure incurred by dynamic scatterers, where N_D is the number of dynamic scatterers, *i.e.*, $\Psi_D = \Psi_D(\tau; v)$, $\tau \in \mathbf{R}^{N_\tau}$, $v \in \mathbf{R}^{N_D}$. $\Theta_D^H \in \mathbf{R}^{N_D \times N_f}$ is the frequency gain to normalize ACF matrix Ψ_D . Similarly, we can compute \mathcal{R}_2 as

$$\mathcal{R}_2 = \Theta_D^H \cdot \mathbf{I}_{N_D} + \Sigma_N(f). \quad (11)$$

$\psi_G(f, t, \tau)$ is irrelevant with t and can be seen as linear combination of Ψ_D . At τ_j , Ψ_D is composed of $\psi_p \in \mathbf{R}^{N_D}$, *i.e.*,

$$\begin{aligned} \Psi_D|_{\tau=\tau_j} &= \Psi_D(\tau = \tau_j; v) \\ &= \psi_p(v; \tau_j), \quad i = 1, \dots, N_D. \end{aligned} \quad (12)$$

Considering a single moving target, we can assume that all the dynamic scatterers contributed by the target share approximately the same speed v_i as the walking speed v . The assumption holds in practice as for human targets, the major reflection energy from the torso dominates that from limbs. Notably, prior DFS-based work implicitly adopted similar assumptions, *e.g.*, hand gesture works usually neglect body motions [35, 85, 88]. To this end, we get $\Psi_D|_{\tau=\tau_j} = \psi_p(v; \tau_j)$. With this, we can compute Eq. (9) as

$$\psi_G(f, \tau) = \widehat{\Theta}_D^H \cdot \Psi_D|_{\tau} = \widehat{\Theta}_D^H \cdot \psi_p(v; \tau), \quad (13)$$

where $\widehat{\Theta}_D^H$ is the broadcast aggregation of Θ_D^H and $\Sigma_N(f)$.

With the above Eq. (13), we bridge the ACF of the CSI and that of sound pressure as a function of speed, for the first time, offering a completely different approach to acoustic speed estimation by calculating the ACF of the CSI measured on commodity audio devices. Practically, with the CSI time series as input, we can use the sample ACF $\tilde{\psi}_G(f, \tau)$, where a noise term $\mu(f, \tau)$ will be added to $\psi_G(f, \tau)$.

Fig. 5 shows the ACF of CSI under different speeds. As can be seen, the shape of $\psi_G(f, \tau)$ well resembles $\psi_p(v; \tau)$ as expected. Thus, to derive the speed v , we can find a reference point to align the calculated $\tilde{\psi}_G(f, \tau)$ to the theoretical $\psi_p(v, \tau)$. In our work, we use the first peak of $\psi_G(f, \tau)$, yet the first valley or their combination will also work. Let x_0 denote the reference point on $\psi_p(v, \tau)$, then the speed can be acquired to solve the optimization problem:

$$\begin{aligned} &\min_v \left| x_0 - \frac{\lambda(f)}{2\pi} v \tau_s \right|, \\ \text{s.t. } &x_0 = \min_x \left\{ x : \frac{d\psi_p(x)}{dx} = 0 \wedge \frac{d^2\psi_p(x)}{dx^2} < 0 \right\}, \end{aligned} \quad (14)$$

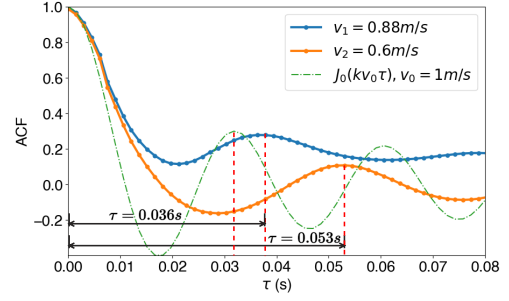


Figure 5: ACF curves for two different speeds and the theoretical function for $v_0 = 1m/s$.

where $\lambda(f)$ represents the wavelength of sound related to its subcarrier frequency f and τ_s is the counterpart of x_0 on $\psi_G(f, \tau)$, *i.e.*, the delay corresponding to the first peak. This is independent from either 2D or 3D model we choose and allows an efficient approach for speed estimation, as we only need to calculate the ACF of the CSI and localize τ_s .

Remarks: ASE is the first to employ the *sound diffusion model* for speed estimation and *comprehensively* integrate it with the acoustic channel. The proposed model fundamentally advances acoustic speed estimation by exploring sound pressure theory and leveraging all multipath reflections. As shown in Fig. 1, Eq. (5) and (6), we leverage all the multipath components and integrate over all directions. This approach diverges completely from traditional DFS methods, marking a new foundation for acoustic speed estimation.

4 ASE DESIGN

This section presents a pipeline of novel techniques that translate our theoretical model into a practical system for robust and accurate speed estimation.

4.1 Baseband Sequence Selection

Transmitted Sequence: CSI is by default not available in acoustic sensing, and we send certain signals to probe the channel. Normally, there are three main types of waveform in acoustic sensing [13]: pure-tone, Pseudo-Noise (PN) code, and FMCW. While FMCW signals are widely used in acoustic sensing [16, 34], they are not standard impulse signals and thus introduce CIR estimation errors. As for the sole impulse signal, the energy of the short-time signal would fade out quickly. Therefore, we seek the PN sequence for CIR estimation in ASE. PN sequence consists of equally-spaced Dirac impulses, signs of which alternate with specific rules. It is a noise-like signal with statistical randomness. We choose Kasami sequence [30] as our sensing waveform, mainly due to its superior orthogonality and tolerance to interference. Particularly, the mutual orthogonality of Kasami sequences is critical to our OTDM design, as detailed in §2.

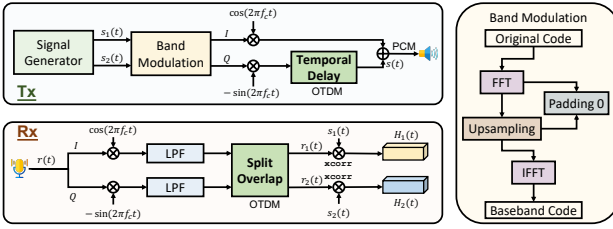


Figure 6: Transmitter and Receiver Design of ASE. Tx: Band modulation (§4.1) and I/Q modulation (§4.2); Rx: Receiver Demodulation (§4.2) and Channel Estimation (§4.1)

Modulation to Inaudible Band: ASE uses only the inaudible sounds for sensing and modulates the sensing signals on the acoustic band of 17 kHz to 24 kHz, the pseudo-ultrasonic band supported by most commodity devices today. Since the PN code including Kasami has a spreading spectrum over the whole band, we should modulate the Kasami sequence to our desired band. The modulation process is shown in Figure 6. The conversion of the full-band signal into a band signal is achieved by either temporal [85] or spectral [58] interpolation. In ASE, we use the frequency domain interpolation. We perform N -point FFT to obtain the frequency domain information, where N is the original length of the sequence. Zero Padding is performed between positive and negative frequency, creating a new sequence of length N_s . Then we perform IFFT to obtain the temporal signal. The band of the interpolated signal is thus transformed to $\frac{N}{N_s}f_s$. For a single-sequence signal, we can multiply it with the carrier signal to move the frequency band towards central frequency f_c . In ASE, we choose $f_c = 20.25\text{kHz}$. We use 63-point Kasami sequences and modulate them to $N_s = 512$, achieving a bandwidth of 5.9kHz. The transmission signal is coded via PCM and decoded at the receiver’s end.

4.2 Transmission Scheme

In this part, we will elaborate our transmission scheme design. We will then describe the channel estimation principles. **Single-Speaker OTDM:** We stack two orthogonal signals as a complex signal and pass it into the I/Q modulator for transmission. Specifically, we can treat the orthogonal sequences $s_1(t)$ and $s_2(t)$ as the real and imaginary part of a complex signal, *i.e.*, $s(t) = s_1(t) + js_2(t)$. To delay $s_2(t)$, we shift the sequence by padding zeros to the front of $s_2(t)$. Practically, however, a speaker can only transmit a single sequence of real signals. To transmit the resultant complex signal over a speaker, we pass it through an I/Q modulator to convert it into a real one. As illustrated in Fig. 6, we additionally multiply $s_1(t)$ and $s_2(t)$ with a carrier signal of orthogonal phase and obtain the modulated real signal: $s(t) = s_1(t) \cos(2\pi f_c t) - s_2(t) \sin(2\pi f_c t)$. With such modulation, the two components remain orthogonal to each other,

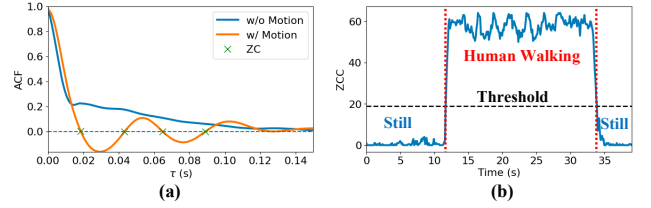


Figure 7: Illustration of Motion Detection. (a) ACF w/ and w/o movement. ACF without motion has considerably lower ZC counts. (b) Extracted ZCC feature to detect motion.

while the modulated signal can be transmitted through a single speaker. At Rx, the received signal is first demodulated by the carrier signal with a low-pass filter (LPF). We can then separate the overlapped signal and estimate the CSI for each sequence at the receiver’s side, as shown in Fig. 6. By doing so, we can obtain two separated signals $r_1(t)$ and $r_2(t)$. Then channel estimation will be performed as follows.

Channel Estimation: To capture the channel properties, we generate the Kasami sequence $s(t)$ of length N_s as the probe signal and transmit it over a speaker. The signal interacts with the environment before arriving at the microphone, where it undergoes scatters in the sound diffusion field. At the receivers end, we acquire $r(t)$ and separate them into $r_1(t)$ and $r_2(t)$, respectively. The CIR $h(t)$ is then estimated as the correlation between them, *i.e.*, $h_i(t) = r_i(t) * s(t)$, $i \in \{1, 2\}$. Then CSI $H_i(f, t)$ is obtained by transforming $h_i(t)$ into the frequency domain via FFT. $H_1(f, t)$ and $H_2(f, t)$ will be then merged using the OTDM scheme to acquire the boosted channel estimation $H(f, t)$, as illustrated in §2.

4.3 Speed Estimation

Now we present how to estimate speed from the CSI time series, given the model described in §3. We devise a robust motion indicator to detect movements. We perform speed estimation when motion is detected. We further enhance frequency diversity to achieve robust speed estimation.

Motion Indicator: A robust motion indicator can help ensure only valid measurements are used for speed estimation, reducing the system overhead while improving estimation accuracy. Therefore, we propose a novel motion indicator called Zero Crossing Count (ZCC) in ASE. As described in Sec. 3, ACF of channel power $\psi_C(f, \tau)$ is the function of moving speed v . When there is no motion, the ACF curve would be overall flat, resulting in no obvious peaks or zero crossings. In contrast, in the case of motion, the ACF will exhibit peaks and valleys, resulting in significantly more zero crossings, as shown in Fig. 7. To identify motion, we can perform Zero Crossing (ZC) analysis on the ACF and count dominant ZCs. Fig. 7 shows an example of the ACF and ZCC values, indicating a clear difference between motive

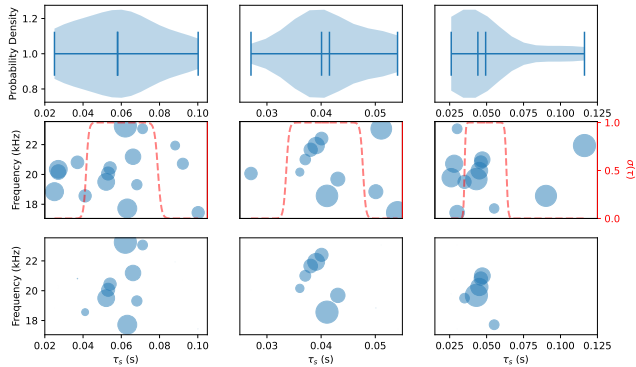


Figure 8: Peak prominence weighting examples. Top: Violin plots of the distribution of the delays of the first peak. Middle: Original weight distribution, where the circle size indicates the weights. The red dashed line represents the fitted $\sigma(\tau)$. Bottom: Adjusted prominence weights.

and still states. Hence, we can find a threshold to reliably detect motion from the ZCC values.

Weighted Subcarrier Combining: Proposed model accounts for all multipath components for speed estimation. Recall Eq. (13), however, the theoretical model estimates speed from one single subcarrier. Given multiple subcarriers available, we can further embrace frequency diversity to boost speed estimation. Instead of performing speed estimation on each subcarrier and fusing the estimates, we propose to properly combine $\hat{\psi}_G(f, t)$ calculated on each subcarrier to enhance the SNR of the speed signal. Formally, we aim to obtain the boosted ACF as $\hat{\psi}_G(\tau) = \sum w(f)\psi_G(f, \tau)$, where

$$\begin{aligned} \max_w \quad & \hat{\psi}_G(\tau_s) = \sum_i w(f_i)\psi_G(f_i, \tau_{s_i}), \\ \text{s.t.} \quad & \sum_i w(f) = 1, w(f) \geq 0, \forall f \in \mathbb{F}, \end{aligned} \quad (15)$$

where \mathbb{F} denotes the subcarrier set. τ_s is the first peak of $\hat{\psi}_G(\tau_s)$. The key is to find optimal weights $w(f)$ for effective combining. The desired goal is to obtain prominent peaks in the ACF for accurate and robust speed estimation. Therefore, we propose a novel weighting method based on the original peak prominence. The idea is that larger weights should be given to the ACF that features more prominent first peaks. Denote $\kappa(t)$ as the prominence of the detected first peak in $\psi(f, \tau)$. Intuitively, we can simply set $w(f) = \kappa(t)$ and combine all subcarriers. However, as shown in Fig. 8, we observe that some ACF may have prominent peaks largely deviated from the centered delay of the majority of peaks. This would enlarge the noise and lower the combined first peak. To this end, we design a compensatory weight decaying algorithm. Specifically, we calculate the mean and median lags of all the identified peaks, and their lower or upper quartiles. We keep the prominence for peaks whose delays between the mean

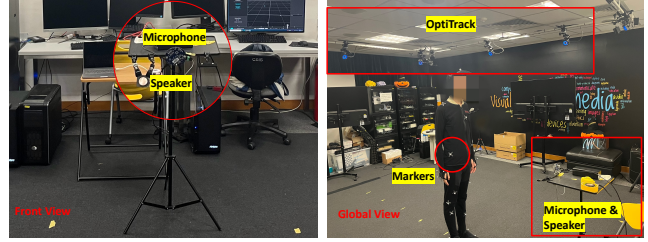


Figure 9: Experiment Setting

and median untouched, reduce the weights for those between the mean/median and the quartiles, and discard those falling outside the quartiles. Therefore, we use a sigmoid function as the decaying curve: $\sigma(\tau) = 1/(1 + \exp(-a(\tau - b)))$, where τ is the peak value and a and b are two parameters that can be fitted. The adjusted prominence values are used as the weights for calculation in Eq. (15).

Frequency Alignment: The weighted combining will enhance the speed signals and reduce the noise, only if the signals are synchronized. However, significant subcarrier frequency variations misalign the ACFs across subcarriers, particularly the first peak, for the same speed. Take two subcarriers on 20 kHz and 24 kHz as an example. Considering a speed $v = 0.5m/s$, the peaks will appear at a delay $\tau = x_0\lambda(f)/2\pi v$. The wavelength $\lambda(f)$ depends on the carrier frequency, and will be 1.715 cm for 20 kHz and 1.429 cm for 24 kHz, leading to two considerably different delays for the first peaks in the respective ACFs. Therefore, we need to eliminate the subcarrier frequency differences and align all the ACFs. We scale the ACF in the lag domain and align them with respect to the first peaks. Particularly, we choose a virtual frequency as a reference, denoted as f_{ref} , and scale the ACF on all subcarriers to the same f_{ref} , i.e., $\psi(f, \tau) \rightarrow \psi(f_{ref}, \tau')$. Recall Eq. (14), we obtain the aligned first peak as, $\tau'_s = f/f_{ref} \cdot \tau_s$. Then the weighted combining can be done on the aligned ACF.

5 IMPLEMENTATION

Hardware: We implement ASE with programmable smart speaker prototype, i.e., a microphone [9], and speaker[4]. Notably, we only **use one microphone channel** in our experiments. The microphone and the speaker are co-located. **Software:** We implement the algorithms of ASE in Python and Matlab. Specifically, we develop a sound playing and recording program with Python and implement the pipeline of processing algorithms with Matlab. We apply 1-s window to compute ACF with a step of 0.1s. We perform motion detection, based ZCC, to determine whether a user is moving and perform speed estimation when motion is detected. Before weighted subcarrier combining, we also perform outlier detection to sift out some abnormal ACFs, which occasionally appears as either a near-linear trend or a zig-zag spikes.

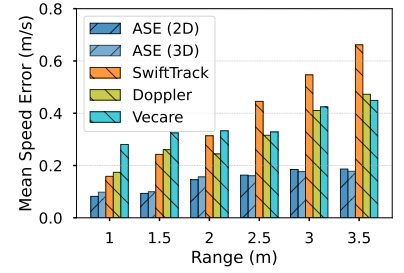
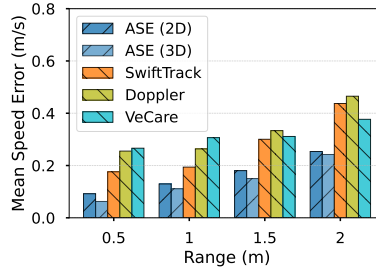
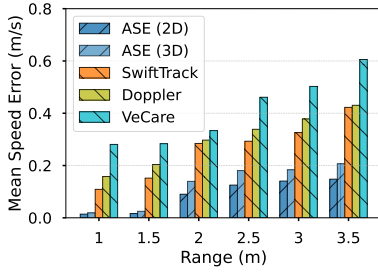


Figure 10: Mean Speed Error of DW

Figure 11: Mean Speed Error of CW

Figure 12: Mean Speed Error of RW

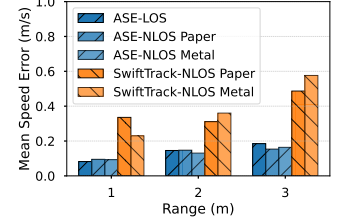
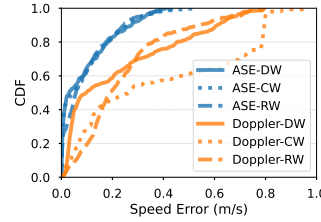
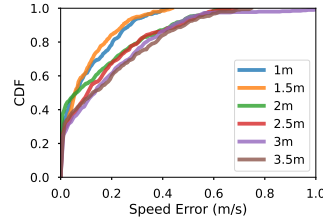
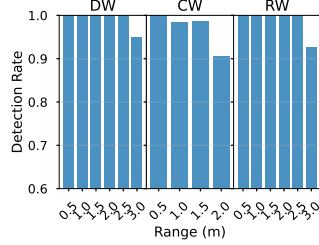


Figure 13: Detection Rate

Figure 14: CDF vs Distances

Figure 15: Walk Means

Figure 16: NLOS Case

6 EXPERIMENTS

As shown in Fig. 9, we mainly conduct our experiment in a 4×4 m room equipped with the OptiTrack [7], which serves as the ground truth. We derive speed from the solved whole-body skeleton coordinates from OptiTrack. We have gained IRB approval by our university for data collection. In total, we have collected over 700 minutes of moving data traces. We evaluate the performance of ASE under various settings. We use mean speed error and detection rate (*i.e.*, how often ASE can reliably detect a speed) as the main evaluation metrics.

6.1 Overall Performance

Our evaluation of ASE considers the coverage and orientation of the audio devices by involving three different scenarios: direct walk (*i.e.*, a straight line towards the devices), circle walk (*i.e.*, around the devices with varying radii) and random walk (*i.e.*, zig-zag walk, back-and-forth walk and run, *etc.*).

Direct Walk (DW): We place the device at the center of one wall in the room. Participants are asked to walk towards the audio device from 1m to 3.5m. We calculate the mean speed error in Fig. 10 and detection rate in Fig. 13. Our results demonstrate that ASE can estimate speeds reliably up to a distance of 3.5 m, with an average speed error of 0.08 m/s. When the object is close, the mean speed error is 0.016 m/s, which increases to 0.14m/s at 3.5m. Our system achieved an average detection rate of 99.0% in the case of direct walking, with a slight degradation to 95.0% at a distance of 3.5m.

Circle Walk (CW): We conduct experiments in a circle-walk scenario. Participants were instructed to walk around the device at varying radii between 0.5m and 2m. The mean error and detection rate are depicted in Fig. 11 and Fig. 13 respectively. While DFS often struggles to estimate speed on

a circular path, ASE achieves a mean speed error of 0.13m/s within 1 meter, 2 times lower than that of DFS.

Random Walk (RW): We comprehensively evaluate the performance of ASE in random walk scenarios. To do so, we let participants move freely within the experimental room, and summarize the results in Fig. 12 and Fig. 13. As seen, our approach achieved an average detection rate of 98.8%, with a perfect detection rate of 100% within 3m. The total average mean error is 0.13m/s, which lowers to 0.08m/s when participants are walking within a shorter range. We also portray the CDF in Fig. 14, which shows a 90%-tile error of less than 0.2m/s. The results demonstrate ASE's robust performance in realistic environments for practical applications.

2D vs 3D model: We evaluate both 2D and 3D models in different scenarios, as illustrated in Fig. 10, Fig. 11 and Fig. 12. The 3D model shows a lower mean speed error of 2.2 cm/s in circle walk scenarios compared to the 2D model. In random walk scenarios, the 3D model is more effective at longer distances. This evaluation underscores the feasibility of both models and their applicability to different scenarios.

6.2 Comparative Study

We compare ASE with three baselines: 1) SwiftTrack [88]: An acoustic speed algorithm for practical fast motion tracking, 2) DFS: A widely used method, implemented based on CAT [38], and 3) VeCare [87]: A recent work of statistical acoustic sensing framework for child presence detection. The former two are DFS-based speed estimation approaches. For a fair comparison, we transmit modulated Zadoff-Chu (ZC) signals as in [88] with the same frame length, *i.e.*, 10ms. We use unmixed CSI and extracted the frequency shift peak in the DFS spectrum for Doppler. We compare baselines under

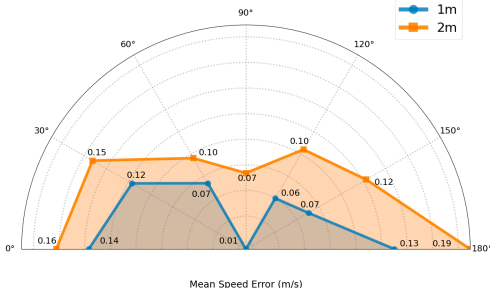


Figure 17: Impact of different directing angles

scenarios in §6.1, and also test the Non-Line-of-Sight (NLoS) condition. We apply the same settings as VeCare.

Different Walk Means: Fig. 10, Fig. 11, and Fig. 12 compare the performance for direct walk, circle walk, and random walk, respectively. While ASE achieves a median error of 0.08m/s in direct walking, SwiftTrack and Doppler yield errors of 0.26m/s and 0.30m/s, respectively. Moreover, ASE significantly surpasses SwiftTrack and Doppler by 68.9% and 101% for circle walk and by 176.7% and 146.2% for random walk. We further depict the CDF of ASE against Doppler in Fig. 15. It shows DFS exhibits poor performance in circle walk while ASE retains consistent performance across various walking means. It is plausible for worse performance of SwiftTrack against Doppler in random walk, given its speed estimation algorithm is tailored for gesture tracking.

Sensing Distance: A unique advantage of ASE is the enlarged sensing coverage, and we verify this by evaluation over different distances, as illustrated in Fig. 10, Fig. 11 and Fig. 12. While the error generally increases with respect to distances for all the methods, ASE consistently outperforms the baseline methods at all distances, with more significant performance gains at larger distances. As shown in Fig. 10, ASE achieves mean speed error less than 0.15m/s at 3.5 m, while SwiftTrack and Doppler soar to 0.42m/s and 0.43m/s, respectively. Overall, both SwiftTrack and Doppler degrade significantly beyond the distance of 1.5m. ASE obtains superior performance because our model leverages all multipath signals, which gets more observations across the room and expands the range to accommodate room-scale sensing.

LoS vs. NLoS: We assess our system in NLoS settings with obstructions like a metal panel or a paper bag in front of the speaker and microphone. Despite sound’s known vulnerability to absorption [60], ASE remains effective in NLoS scenarios, exhibiting an average error rate of 0.13m/s and a standard deviation of merely 0.003m/s, as illustrated in Fig. 16. In contrast, the performance of SwiftTrack drops by 14.4% and 11.2% under metal and paper obstructions, respectively. We benefit from the effective use of multipath reflections, which is particularly helpful in NLoS scenarios.

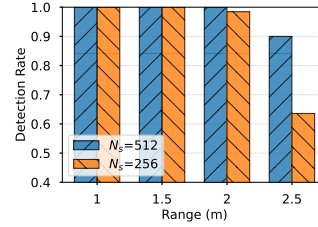


Figure 18: Impact of sequence lengths

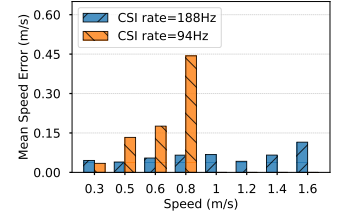


Figure 19: Impact of different CSI rates

Comparison with VeCare: VeCare includes a statistical framework for presence detection, which mentions speed components. We implement the algorithm and evaluate in three scenarios. As shown in Fig. 10, Fig. 11 and Fig. 12, the performance of VeCare is much worse than our ASE. Notably, the performance of ASE is 149.9% better than VeCare in random walk scenarios. VeCare, which extrapolates Wi-Fi sensing methods without comprehensive modeling, is not targeted for speed estimation and does not include specific designs. These results highlight the novelty and superiority of our speed estimation techniques and theoretical model.

6.3 Benchmark Study

We present a micro-benchmark study of ASE in this section.

Different Orientations: We evaluate the impact of different walking orientations at various angles with respect to the audio devices. We evaluate different angles, from 0° to 180° with an increase of 30°, where 90° is defined as facing directly towards the device. As illustrated in Fig. 17, the smallest speed error is observed at 90°. The errors increase as the orientation shifts away from 90° towards both sides, yet are still acceptable even when at 0° or 180°.

Sound Level: We modulate the transmission signal to the inaudible band to minimize interference with human hearing for daily use as detailed in Sec. 5, rendering the sound nearly inaudible. To evaluate the impact of different sound levels, we transmit signals at sound pressure levels of 33.4dB, 35.3dB, 36.7dB, 38.2dB, and 41.7dB, respectively. As shown in Fig. 21, the results indicate that the mean speed error decreases as the sound volume increases, as does the detection rate. Notably, our system’s maximum sound pressure of 41.7dB is significantly lower than most previous acoustic sensing studies [40, 64, 85, 87]. Despite the sound leakage problem on commodity devices [33], the sound noise of our system can be fairly neglected in commonly used settings.

Amplitude of Kasami Sequence: Besides volume of the device, the sound power is also determined by the amplitude of the original sequence. We hereby experiment with different amplitudes, shown in Fig. 22. This is not the final amplitude

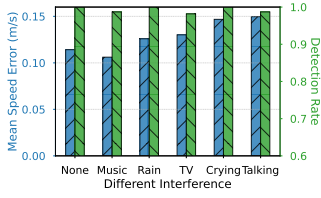


Figure 20: Impact of different interference sources

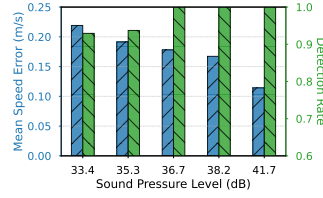


Figure 21: Impact of different sound volume level

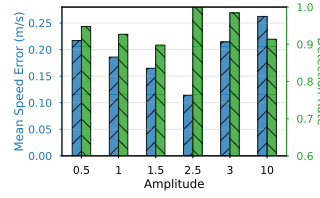


Figure 22: Impact of amplitudes of original sequence

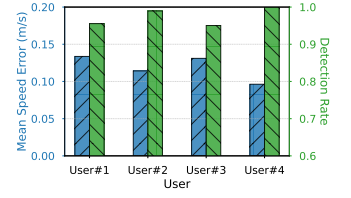


Figure 23: Performance for different users

of the transmitted signal, as it must go through band modulation and PCM before transmission. As seen, the performance decreases first and then increases as amplitudes increase, and an amplitude of 2.5 strikes the best for both speed accuracy and detection rate. Amplitudes smaller than 2.5 will result in low sound power and thus large errors, while overlarge amplitudes will lead to distortions of the signal [33] due to the hardware limitation. In our case, sounds with amplitudes larger than 2.5 would be clipped off. Hence, we choose 2.5 as the amplitude of the original PN sequence.

Interferences: We also conduct experiments to evaluate the performance under different interference sources. We choose common sources of interference in indoor environments, including music, rain, TV broadcasting, baby crying, and human talking, illustrated in Fig. 20. This indicates that our system is robust to noise and interference, and can accurately estimate the speed even in the presence of interference.

Sequence Lengths: We then study the influence of different sequence lengths N_s . As discussed above, the sequence length impacts the sensing coverage and CSI rate. When the sequence length is reduced, the CSI rate would increase, but the sensing coverage would diminish simultaneously. To investigate it, we conduct experiments using sequence lengths of 512 and 256 and mainly examine the detection rate to study the coverage. As shown in Fig. 18, using both lengths achieves great performance for small coverage, *e.g.*, within 1.5 m. However, the detection rate for the sequence length of 256 drops significantly at larger distances of 2m and 2.5m. Particularly, at a distance of 2.5m, the detection rate drops to 63.6% for $N_s = 256$ while the rate still remains at 99% for $N_s = 512$. ASE defaults to $N_s = 512$ to strike a balance between sensing coverage and CSI rate.

CSI Rate: We now study how CSI rates will impact the performance for different speeds. To control the moving speed, we use a programmable rail track with a plate on it. We test with speeds of 0.3m/s to 1.6m/s, and compare the performance with a CSI rate of 94 Hz and 188 Hz, respectively. We apply OTDM scheme to achieve the CSI rate of 188 Hz. As shown in Fig. 19, a low CSI rate cannot measure large speeds and will produce large errors. The mean errors for speeds of 0.6m/s and 0.8m/s with a CSI rate of 94Hz are 0.18m/s and 0.44m/s, respectively. Comparatively, the corresponding

errors with that of 188Hz are 0.055m/s and 0.066m/s, respectively. Notably, our system maintains a relatively low average error of 0.11m/s even at 1.6m/s. Overall, the results clearly demonstrate the need for a sufficient CSI rate for speed estimation and justify the effectiveness of the proposed OTDM scheme. In ASE, we can hold speed up to 1.6m/s using single-speaker, adequate for capturing indoor walk speed.

Different Subcarrier Combining Weight: We test different subcarrier combining weight method. Our results show using prominence as the weight leads to a mean speed error of 0.13m/s, whereas MS results in an error of 0.19m/s. Besides, we compare different weight decaying algorithms. We observe a 15% decrease in mean speed error when applying sigmoid weight decay. These results confirm the effectiveness of our subcarrier combination weight in ASE.

Different Location: To test ASE in different environments, we perform experiment in different locations, including a conference room and an office. The experiment subject is walking randomly within 4m range. We have achieved 100% and 97.13% detection rate in these scenarios. Therefore, our system can adapt to different indoor environments.

Different Users: We also examine how ASE performs for different users. We recruit four volunteers and let them walk freely with varying speeds, orientations, and trajectories. The results are shown in Fig. 23, which shows a mean error of 0.12m/s and an average detection rate of 97.4%, with only marginal differences among different users.

System Overhead: We mainly employ MacBook 2021 to run the experiments. Our statistical algorithms are lightweight, with an average latency of 2.32s over 40s acoustic data. The channel estimation takes 0.20s on average and the weight decay and combination accounts for 0.41s.

6.4 Case Study

We present three case studies to showcase various ASE-enabled applications.

Human Activity Recognition: Speed profiles act as the core of human activity recognition [19, 45, 51, 55, 79]. As shown in Fig. 24, the speed profiles (the dashed lines) generated by ASE can effectively distinguish different daily activities such as standing up, sitting down, and picking up objects. For instance, the speed profile of standing up shows a slower increase compared to sitting down. Picking up an

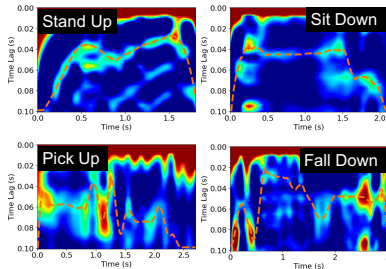


Figure 24: Speed profile of different human activities

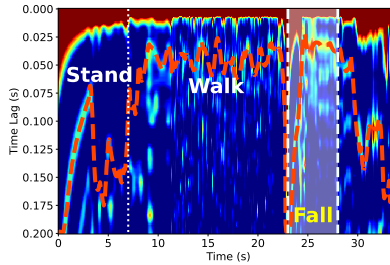


Figure 25: Speed profile of continuous activities

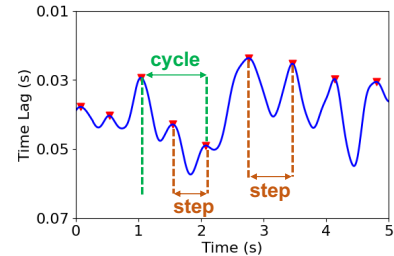


Figure 26: Gait step and Cycle

object, however, forms a 'valley' in the profile, reflecting the bending and rising motion. Fig. 25 provides an example of recognizing different activities through continuous monitoring. We keep it as a future direction to recognize different activities with ASE deployed on commodity smart speakers. **Fall Detection:** Fall detection is a vital yet challenging task. Passive speed estimation provides an effective way to detect falls [26, 29, 37, 90], mainly because falls induce a distinct speed pattern compared to normal daily activities. As shown in Fig. 24 and Fig. 25, a fall induces a unique pattern in the ACF matrix. The speed changes rapidly from a lower rate to a significantly higher rate within a brief period, yielding a large instantaneous acceleration. Following speed suggests further movement on the ground, before eventually decreasing to zero. Based on these observations, we employ deep learning for proof-of-concept fall detection. As the ACF matrix contains speed information, we leverage pretrained MobileNet-v2 [54] as the ACF matrix encoder to classify the fall events. In total, we have 305 samples, with 175 representing fall events. We achieve the F-1 score of 0.92, demonstrating the effectiveness of ASE for feature extractions.

Gait Analysis: Gait analysis is important in healthcare, especially for patients with Parkinson's disease [11, 17, 81]. Intuitively, the walking speeds estimated by ASE allow us to perform gait analysis. As a proof-of-concept, we recognize gait steps and cycles by detecting the peak in the speed profile, as shown in Fig. 26. Our analysis of 10 traces reports an average gait cycle time of 1.00s with a variance of 1.2ms, demonstrating the potential of ASE for gait applications.

7 DISCUSSIONS

Multiple speed: ASE assumes the human body shares the same speed v for walk speed estimation, which is also adopted by many other works [35, 44, 88]. Eq. (12) suggests the potential to decompose the ACFs to account for varying speeds, which indicates an opportunity for future research to refine speed estimation by considering multiple speed scenarios.

Multi-target Scenario: Current ASE is not designed for multi-person scenarios. In most cases, indoor walking speed downstream tasks, such as fall detection and gait monitoring,

involve single person. Audio devices enable the interaction in real-time and alarm when abnormal conditions are detected. Therefore, ASE can already foster many applications. Yet it is also potential extend it to multi-person sensing in the future, e.g., by separating multipath signals for different ranges. **Multiple Speakers:** In ASE, we use OTDM with a single speaker and two channels, offering practical room-scale sensing. While this setup is common, OTDM can be extended to multiple speakers with advanced modulation. Future work can explore OTDM+OFDM design for higher CSI rates.

8 RELATED WORKS

Acoustic Sensing: Acoustic sensing has been extensively explored recently and realize multiple applications, including indoor localization [22, 36, 39, 41], fine-grained gesture tracking [35, 38, 43, 58, 63, 70, 82, 83, 88], vital signs monitoring [34, 48, 62, 64, 65, 68], silent speech enhancement [21, 57], sound source localization [18, 56, 67], and communication [15, 89]. VeCare [87] introduces statistical acoustic sensing for presence detection, by extrapolating statistical WiFi sensing. However, it neither constructs the comprehensive model nor considers the fundamental differences between acoustic and electromagnetic waves. Conversely, ASE integrates a novel sound diffusion model with the acoustic channel for speed estimation for the first time. Additionally, we propose the first-of-its-kind OTDM design to increase the CSI rate, enabling the high speed estimation with robust performance. **Speed Estimation:** Speed is vital information in human sensing, and has been exploited in various applications like fall detection [28, 37, 46, 71], interactive games [50], gait monitoring [61, 74, 81], and localization [41, 49]. Speed estimation, however, is a challenging and enduring task. Camera-based approach, such as VICON [10], requires professional device and specialized calibration, which cannot be used in ubiquitous settings. In wireless sensing, speed is generally derived using DFS, regardless of Wi-Fi [49, 59, 78], acoustic [38, 38, 56, 58, 67, 84, 88], or mmWave radar [12, 76] signals. Despite the advances in statistical wireless sensing [74, 86], sound waves and EM waves differ in nature, and acoustic speed estimation incurs different challenges. We build the

acoustic diffusion speed estimation model plus OTDM design, a new way of acoustic speed estimation.

9 CONCLUSIONS

In this paper, we present *ASE*, a system for acoustic speed estimation. We propose a novel OTDM scheme to achieve a higher CSI rate for speed estimation. Inspired by the sound diffusion field, we establish a comprehensive theoretical model that enables full speed estimation from the spatial correlation of sounds. We extensively evaluate *ASE* on commodity devices, which achieves an average accuracy of 13 cm/s for normal walking speed estimation. Overall, the proposed *ASE* goes beyond the DFS-based paradigm and can open up new directions in acoustic sensing.

REFERENCES

- [1] 2021. Amazon.com: Echo Smart Speakers & Displays: Amazon Devices & Accessories: Smart Speakers, Smart Displays & More. <https://www.amazon.com/smart-home-devices/b?ie=UTF8&node=9818047011>
- [2] 2021. A home that knows how to help. <https://home.google.com/welcome/>
- [3] 2021. X4M03 – laonuri.com. <https://www.laonuri.com/product/x4m03/>
- [4] 2022. Speakers & Receivers | AS05308AS-R. <https://puiaudio.com/product/speakers-and-receivers/AS05308AS-R>
- [5] 2023. Intel® Wi-Fi 6 AX200 (Gig+) - Product Specifications. <https://www.intel.com/content/www/us/en/products/sku/189347/intel-wifi-6-ax200-gig/specifications.html>
- [6] 2023. IWR1843 data sheet, product information and support | TI.com. <https://www.ti.com/product/IWR1843>
- [7] 2023. Motion Capture Systems. <http://optitrack.com/index.html>
- [8] 2023. Support for Intel® WiFi Link 5300. <https://www.intel.com/content/www/us/en/support/products/70971/network-and-i-o/wireless-networking/legacy-intel-wireless-products/intel-wireless-series/intel-wifi-link-5300.html>
- [9] 2023. USB Audio Streaming: UMA-8-SP USB mic array. <https://www.minidsp.com/products/usb-audio-interface/uma-8-sp-detail>
- [10] 2023. Vicon | Award Winning Motion Capture Systems. <https://www.vicon.com/>
- [11] MD Akhtaruzzaman, Amir Akramin Shafie, and Md Raisuddin Khan. 2016. Gait analysis: Systems, technologies, and importance. *Journal of Mechanics in Medicine and Biology* 16, 07 (2016), 1630003.
- [12] Alejandro Blanco, Pablo Jiménez Mateo, Francesco Gringoli, and Joerg Widmer. 2022. Augmenting mmWave localization accuracy through sub-6 GHz on off-the-shelf devices. In *Proceedings of the 20th Annual International Conference on Mobile Systems, Applications and Services*. 477–490.
- [13] Chao Cai, Rong Zheng, and Jun Luo. 2022. Ubiquitous acoustic sensing on commodity iot devices: A survey. *IEEE Communications Surveys & Tutorials* 24, 1 (2022), 432–454.
- [14] Huijie Chen, Fan Li, and Yu Wang. 2017. EchoTrack: Acoustic device-free hand tracking on smart phones. In *IEEE INFOCOM 2017 - IEEE Conference on Computer Communications*. 1–9. <https://doi.org/10.1109/INFOCOM.2017.8057101>
- [15] Tuochao Chen, Justin Chan, and Shyamnath Gollakota. 2022. Underwater messaging using mobile devices. In *Proceedings of the ACM SIGCOMM 2022 Conference*. 545–559.
- [16] Haiming Cheng and Wei Lou. 2021. Push the Limit of Device-Free Acoustic Sensing on Commercial Mobile Devices. In *IEEE INFOCOM 2021 - IEEE Conference on Computer Communications*. 1–10. <https://doi.org/10.1109/INFOCOM42981.2021.9488703> ISSN: 2641-9874.
- [17] Ting-Hui Chiang, Yi-Juan Su, Huan-Ruei Shiu, and Yu-Chee Tseng. 2020. 3D Gait Tracking by Acoustic Doppler Effects. In *2020 42nd Annual International Conference of the IEEE Engineering in Medicine & Biology Society (EMBC)*. IEEE, 3146–3149.
- [18] Tingchao Fan, Huangwei Wu, Meng Jin, Tao Chen, Longfei Shangguan, Xinbing Wang, and Chenghu Zhou. 2023. Towards Spatial Selection Transmission for Low-end IoT devices with SpotSound. In *Proceedings of the 29th Annual International Conference on Mobile Computing and Networking*.
- [19] Andrea Ferlini, Dong Ma, Robert Harle, and Cecilia Mascolo. 2021. EarGate: gait-based user identification with in-ear microphones. In *Proceedings of the 27th Annual International Conference on Mobile Computing and Networking*. 337–349.
- [20] Stacy Fritz and Michelle Lusardi. 2009. White paper: “walking speed: the sixth vital sign”. *Journal of geriatric physical therapy* 32, 2 (2009), 2–5.
- [21] Yongjian Fu, Shuning Wang, Linghui Zhong, Lili Chen, Ju Ren, and Yaoxue Zhang. 2022. SVoice: Enabling Voice Communication in Silence via Acoustic Sensing on Commodity Devices. In *Proceedings of the 20th ACM Conference on Embedded Networked Sensor Systems*. 622–636.
- [22] Zihui Gao, Ang Li, Dong Li, Jialin Liu, Jie Xiong, Yu Wang, Bing Li, and Yiran Chen. 2022. Mom: Microphone based 3d orientation measurement. In *2022 21st ACM/IEEE International Conference on Information Processing in Sensor Networks (IPSN)*. IEEE, 132–144.
- [23] Arindam Ghosh, Amartya Chakraborty, Dhruv Chakraborty, Mousumi Saha, and Sujoy Saha. 2019. UltraSense: A non-intrusive approach for human activity identification using heterogeneous ultrasonic sensor grid for smart home environment. *Journal of Ambient Intelligence and Humanized Computing* (2019), 1–22.
- [24] Yanbin Gong, Qian Zhang, Bobby H.P. NG, and Wei Li. 2022. BreathMentor: Acoustic-based Diaphragmatic Breathing Monitor System. *Proceedings of the ACM on Interactive, Mobile, Wearable and Ubiquitous Technologies* 6, 2 (July 2022), 53:1–53:28. <https://doi.org/10.1145/3534595>
- [25] Daniel Halperin, Wenjun Hu, Anmol Sheth, and David Wetherall. 2011. Tool release: Gathering 802.11 n traces with channel state information. *ACM SIGCOMM computer communication review* 41, 1 (2011), 53–53.
- [26] Yuqian Hu, Feng Zhang, Chenshu Wu, Beibei Wang, and KJ Ray Liu. 2020. A WiFi-based passive fall detection system. In *ICASSP 2020-2020 IEEE International Conference on Acoustics, Speech and Signal Processing (ICASSP)*. IEEE, 1723–1727.
- [27] Yuqian Hu, Feng Zhang, Chenshu Wu, Beibei Wang, and KJ Ray Liu. 2021. DeFall: Environment-independent passive fall detection using WiFi. *IEEE Internet of Things Journal* 9, 11 (2021), 8515–8530.
- [28] Yuqian Hu, Feng Zhang, Chenshu Wu, Beibei Wang, and K. J. Ray Liu. 2020. A WiFi-Based Passive Fall Detection System. In *ICASSP 2020 - 2020 IEEE International Conference on Acoustics, Speech and Signal Processing (ICASSP)*. IEEE, Barcelona, Spain, 1723–1727. <https://doi.org/10.1109/ICASSP40776.2020.9054753>
- [29] Sijie Ji, Yaxiong Xie, and Mo Li. 2022. SiFall: Practical Online Fall Detection with RF Sensing. In *Proceedings of the 20th ACM Conference on Embedded Networked Sensor Systems*. 563–577.
- [30] Tadao Kasami. 1966. *WEIGHT DISTRIBUTION FORMULA FOR SOME CLASS OF CYCLIC CODES*. Technical Report. Defense Technical Information Center, Fort Belvoir, VA. <https://doi.org/10.21236/AD0632574>
- [31] Heinrich Kuttruff. 2000. *Room acoustics*. (2000). Publisher: Spon press UK.
- [32] Robert B Leighton and Matthew Sands. 1965. *The Feynman lectures on physics*. Addison-Wesley Boston, MA, USA.

- [33] Dong Li, Shirui Cao, Sunghoon Ivan Lee, and Jie Xiong. 2022. Experience: practical problems for acoustic sensing. In *Proceedings of the 28th Annual International Conference on Mobile Computing And Networking*. 381–390.
- [34] Dong Li, Jialin Liu, Sunghoon Ivan Lee, and Jie Xiong. 2022. LASense: Pushing the Limits of Fine-grained Activity Sensing Using Acoustic Signals. *Proceedings of the ACM on Interactive, Mobile, Wearable and Ubiquitous Technologies* 6, 1 (March 2022), 21:1–21:27.
- [35] Dong Li, Jialin Liu, Sunghoon Ivan Lee, and Jie Xiong. 2022. Room-Scale Hand Gesture Recognition Using Smart Speakers. In *Proceedings of the 20th ACM Conference on Embedded Networked Sensor Systems*. 462–475.
- [36] Jie Lian, Jiadong Lou, Li Chen, and Xu Yuan. 2021-01-01. EchoSpot: Spotting Your Locations via Acoustic Sensing. *Proceedings of the ACM on Interactive, Mobile, Wearable and Ubiquitous Technologies* 5, 3 (Sept. 2021-01-01), 113:1–113:21. <https://doi.org/10.1145/3478095>
- [37] Jie Lian, Xu Yuan, Ming Li, and Nian-Feng Tzeng. 2021. Fall Detection via Inaudible Acoustic Sensing. *Proceedings of the ACM on Interactive, Mobile, Wearable and Ubiquitous Technologies* 5, 3 (Sept. 2021), 1–21. <https://doi.org/10.1145/3478094>
- [38] Wenguang Mao, Jian He, and Lili Qiu. 2016. CAT: high-precision acoustic motion tracking. In *Proceedings of the 22nd Annual International Conference on Mobile Computing and Networking*. ACM, New York City New York, 69–81. <https://doi.org/10.1145/2973750.2973755>
- [39] Wenguang Mao, Wei Sun, Mei Wang, and Lili Qiu. 2020. DeepRange: Acoustic Ranging via Deep Learning. *Proceedings of the ACM on Interactive, Mobile, Wearable and Ubiquitous Technologies* 4, 4 (Dec. 2020), 1–23. <https://doi.org/10.1145/3432195>
- [40] Wenguang Mao, Mei Wang, and Lili Qiu. 2018. AIM: Acoustic Imaging on a Mobile. In *Proceedings of the 16th Annual International Conference on Mobile Systems, Applications, and Services*. ACM, Munich Germany, 468–481. <https://doi.org/10.1145/3210240.3210325>
- [41] Wenguang Mao, Zaiwei Zhang, Lili Qiu, Jian He, Yuchen Cui, and Sangki Yun. 2017. Indoor follow me drone. In *Proceedings of the 15th annual international conference on mobile systems, applications, and services*. 345–358.
- [42] Addie Middleton, Stacy L Fritz, and Michelle Lusardi. 2015. Walking speed: the functional vital sign. *Journal of aging and physical activity* 23, 2 (2015), 314–322.
- [43] Rajalakshmi Nandakumar, Vikram Iyer, Desney Tan, and Shyamnath Gollakota. 2016. FingerIO: Using Active Sonar for Fine-Grained Finger Tracking. In *Proceedings of the 2016 CHI Conference on Human Factors in Computing Systems*. ACM, San Jose California USA, 1515–1525. <https://doi.org/10.1145/2858036.2858580>
- [44] Kai Niu, Xuanzhi Wang, Fusang Zhang, Rong Zheng, Zhiyun Yao, and Daqing Zhang. 2022. Rethinking Doppler effect for accurate velocity estimation with commodity WiFi devices. *IEEE Journal on Selected Areas in Communications* 40, 7 (2022), 2164–2178.
- [45] Xiaomin Ouyang, Xian Shuai, Jiayu Zhou, Ivy Wang Shi, Zhiyuan Xie, Guoliang Xing, and Jianwei Huang. 2022. Cosmo: contrastive fusion learning with small data for multimodal human activity recognition. In *Proceedings of the 28th Annual International Conference on Mobile Computing And Networking*. 324–337.
- [46] Sameera Palipana, David Rojas, Piyush Agrawal, and Dirk Pesch. 2018. FallDeFi: Ubiquitous Fall Detection using Commodity Wi-Fi Devices. *Proceedings of the ACM on Interactive, Mobile, Wearable and Ubiquitous Technologies* 1, 4 (Jan. 2018), 1–25. <https://dl.acm.org/doi/10.1145/3161183>
- [47] Allan D Pierce. 2019. *Acoustics: an introduction to its physical principles and applications*. Springer.
- [48] Kun Qian, Chenshu Wu, Fu Xiao, Yue Zheng, Yi Zhang, Zheng Yang, and Yunhao Liu. 2018. Acousticcardiogram: Monitoring Heartbeats using Acoustic Signals on Smart Devices. In *IEEE INFOCOM 2018 - IEEE Conference on Computer Communications*. IEEE, Honolulu, HI, 1574–1582. <https://doi.org/10.1109/INFOCOM.2018.8485978>
- [49] Kun Qian, Chenshu Wu, Yi Zhang, Guidong Zhang, Zheng Yang, and Yunhao Liu. 2018. Widar2. 0: Passive human tracking with a single Wi-Fi link. In *Proceedings of the 16th Annual International Conference on Mobile Systems, Applications, and Services*. 350–361.
- [50] Kun Qian, Chenshu Wu, Zimu Zhou, Yue Zheng, Zheng Yang, and Yunhao Liu. 2017. Inferring motion direction using commodity wi-fi for interactive exergames. In *Proceedings of the 2017 CHI conference on human factors in computing systems*. 1961–1972.
- [51] Hossein Raeis, Mohammad Kazemi, and Shervin Shirmohammadi. 2021. Human activity recognition with device-free sensors for well-being assessment in smart homes. *IEEE Instrumentation & Measurement Magazine* 24, 6 (2021), 46–57.
- [52] Line Jee Hartmann Rasmussen, Avshalom Caspi, Antony Ambler, Jonathan M Broadbent, Harvey J Cohen, Tracy d’Arbeloff, Maxwell Elliott, Robert J Hancox, HonaLee Harrington, Sean Hogan, et al. 2019. Association of neurocognitive and physical function with gait speed in midlife. *JAMA network open* 2, 10 (2019), e1913123–e1913123.
- [53] Andrea L Rosso, Joe Verghese, Andrea L Metti, Robert M Boudreau, Howard J Aizenstein, Stephen Kritchevsky, Tamara Harris, Kristine Yaffe, Suzanne Satterfield, Stephanie Studenski, et al. 2017. Slowing gait and risk for cognitive impairment: the hippocampus as a shared neural substrate. *Neurology* 89, 4 (2017), 336–342.
- [54] Mark Sandler, Andrew Howard, Menglong Zhu, Andrey Zhmoginov, and Liang-Chieh Chen. 2018. Mobilenetv2: Inverted residuals and linear bottlenecks. In *Proceedings of the IEEE conference on computer vision and pattern recognition*. 4510–4520.
- [55] Dakun Shen, Ian Markwood, Dan Shen, and Yao Liu. 2018. Virtual safe: Unauthorized walking behavior detection for mobile devices. *IEEE Transactions on Mobile Computing* 18, 3 (2018), 688–701.
- [56] Sheng Shen, Dagan Chen, Yu-Lin Wei, Zhijian Yang, and Romit Roy Choudhury. 2020. Voice localization using nearby wall reflections. In *Proceedings of the 26th Annual International Conference on Mobile Computing and Networking*. ACM, London United Kingdom, 1–14. <https://doi.org/10.1145/3372224.3380884>
- [57] Ke Sun and Xinyu Zhang. 2021. UltraSE: single-channel speech enhancement using ultrasound. In *Proceedings of the 27th Annual International Conference on Mobile Computing and Networking*. ACM, New Orleans Louisiana, 160–173.
- [58] Ke Sun, Ting Zhao, Wei Wang, and Lei Xie. 2018. VSkin: Sensing Touch Gestures on Surfaces of Mobile Devices Using Acoustic Signals. In *Proceedings of the 24th Annual International Conference on Mobile Computing and Networking*. ACM, New Delhi India, 591–605. <https://doi.org/10.1145/3241539.3241568>
- [59] Li Sun, Souvik Sen, Dimitrios Koutsonikolas, and Kyu-Han Kim. 2015. Widraw: Enabling hands-free drawing in the air on commodity wifi devices. In *Proceedings of the 21st Annual International Conference on Mobile Computing and Networking*. 77–89.
- [60] Xiaoning Tang and Xiong Yan. 2017. Acoustic energy absorption properties of fibrous materials: A review. *Composites Part A: Applied Science and Manufacturing* 101 (2017), 360–380.
- [61] M. Umair Bin Altaf, Taras Butko, and Biing-Hwang Juang. 2015. Acoustic Gaits: Gait Analysis With Footstep Sounds. *IEEE Transactions on Biomedical Engineering* 62, 8 (Aug. 2015), 2001–2011. <https://doi.org/10.1109/TBME.2015.2410142>
- [62] Haoran Wan, Shuyu Shi, Wenyu Cao, Wei Wang, and Guihai Chen. 2021. RespTracker: Multi-user Room-scale Respiration Tracking with Commercial Acoustic Devices. In *IEEE INFOCOM 2021 - IEEE Conference on Computer Communications*. IEEE, Vancouver, BC, Canada, 1–10. <https://doi.org/10.1109/INFOCOM42981.2021.9488881>

- [63] Anran Wang and Shyamnath Gollakota. 2019. MilliSonic: Pushing the Limits of Acoustic Motion Tracking. In *Proceedings of the 2019 CHI Conference on Human Factors in Computing Systems*. ACM, Glasgow Scotland Uk, 1–11. <https://doi.org/10.1145/3290605.3300248>
- [64] Anran Wang, Jacob E. Sunshine, and Shyamnath Gollakota. 2019. Contactless Infant Monitoring using White Noise. In *The 25th Annual International Conference on Mobile Computing and Networking*. ACM, Los Cabos Mexico, 1–16. <https://doi.org/10.1145/3300061.3345453>
- [65] Lei Wang, Tao Gu, Wei Li, Haipeng Dai, Yong Zhang, Dongxiao Yu, Chenren Xu, and Daqing Zhang. 2023. DF-Sense: Multi-user Acoustic Sensing for Heartbeat Monitoring with Dualforming. In *Proceedings of the 21st Annual International Conference on Mobile Systems, Applications and Services*. 1–13.
- [66] Lei Wang, Wei Li, Ke Sun, Fusang Zhang, Tao Gu, Chenren Xu, and Daqing Zhang. 2022. Loear: Push the range limit of acoustic sensing for vital sign monitoring. *Proceedings of the ACM on Interactive, Mobile, Wearable and Ubiquitous Technologies* 6, 3 (2022), 1–24.
- [67] Mei Wang and Wei Sun. 2021. MAVL: Multiresolution Analysis of Voice Localization. In *Proc. of NSDI* (2021).
- [68] Tianben Wang, Daqing Zhang, Yuanqing Zheng, Tao Gu, Xingshe Zhou, and Bernadette Dorizzi. 2018. C-FMCW Based Contactless Respiration Detection Using Acoustic Signal. *Proceedings of the ACM on Interactive, Mobile, Wearable and Ubiquitous Technologies* 1, 4 (Jan. 2018), 1–20. <https://doi.org/10.1145/3161188>
- [69] Wei Wang, Alex X Liu, Muhammad Shahzad, Kang Ling, and Sanglu Lu. 2015. Understanding and modeling of wifi signal based human activity recognition. In *Proceedings of the 21st annual international conference on mobile computing and networking*. 65–76.
- [70] Wei Wang, Alex X. Liu, and Ke Sun. 2016. Device-free gesture tracking using acoustic signals. In *Proceedings of the 22nd Annual International Conference on Mobile Computing and Networking (MobiCom '16)*. Association for Computing Machinery, New York, NY, USA, 82–94. <https://doi.org/10.1145/2973750.2973764>
- [71] Yuxi Wang, Kaishun Wu, and Lionel M. Ni. 2017. WiFall: Device-Free Fall Detection by Wireless Networks. *IEEE Transactions on Mobile Computing* 16, 2 (Feb. 2017), 581–594.
- [72] Ziqi Wang, Zhe Chen, Akash Deep Singh, Luis Garcia, Jun Luo, and Mani B Srivastava. 2020. Uwhear: through-wall extraction and separation of audio vibrations using wireless signals. In *Proceedings of the 18th Conference on Embedded Networked Sensor Systems*. 1–14.
- [73] Chenshu Wu, Beibei Wang, Oscar C Au, and KJ Ray Liu. 2022. Wi-Fi Can Do More: Toward Ubiquitous Wireless Sensing. *IEEE Communications Standards Magazine* 6, 2 (2022), 42–49.
- [74] Chenshu Wu, Feng Zhang, Yuqian Hu, and K. J. Ray Liu. 2021. GaitWay: Monitoring and Recognizing Gait Speed Through the Walls. *IEEE Transactions on Mobile Computing* 20, 6 (June 2021), 2186–2199.
- [75] Chenshu Wu, Feng Zhang, Yuqian Hu, and KJ Ray Liu. 2020. GaitWay: Monitoring and recognizing gait speed through the walls. *IEEE Transactions on Mobile Computing* 20, 6 (2020), 2186–2199.
- [76] Chenshu Wu, Feng Zhang, Beibei Wang, and KJ Ray Liu. 2020. mmTrack: Passive multi-person localization using commodity millimeter wave radio. In *IEEE INFOCOM 2020-IEEE Conference on Computer Communications*. IEEE, 2400–2409.
- [77] Binbin Xie, Minhao Cui, Deepak Ganesan, Xiangru Chen, and Jie Xiong. 2023. Boosting the Long Range Sensing Potential of LoRa. In *Proceedings of the 21st Annual International Conference on Mobile Systems, Applications and Services*. 177–190.
- [78] Jie Xiong and Kyle Jamieson. 2013. {ArrayTrack}: A {Fine-Grained} indoor location system. In *10th USENIX Symposium on Networked Systems Design and Implementation (NSDI 13)*. 71–84.
- [79] Huatao Xu, Pengfei Zhou, Rui Tan, and Mo Li. 2023. Practically Adopting Human Activity Recognition. In *Proceedings of the 29th Annual International Conference on Mobile Computing and Networking*.
- [80] Wei Xu, ZhiWen Yu, Zhu Wang, Bin Guo, and Qi Han. 2019. AcousticID: gait-based human identification using acoustic signal. *Proceedings of the ACM on Interactive, Mobile, Wearable and Ubiquitous Technologies* 3, 3 (2019), 1–25.
- [81] Wei Xu, ZhiWen Yu, Zhu Wang, Bin Guo, and Qi Han. 2019. AcousticID: Gait-based Human Identification Using Acoustic Signal. *Proceedings of the ACM on Interactive, Mobile, Wearable and Ubiquitous Technologies* 3, 3 (Sept. 2019), 1–25.
- [82] Yilin Yang, Xin Li, Zhengkun Ye, Yan Wang, and Yingying Chen. 2023. BioCase: Privacy Protection via Acoustic Sensing of Finger Touches on Smartphone Case Mini-Structures. In *Proceedings of the 21st Annual International Conference on Mobile Systems, Applications and Services*. 397–409.
- [83] Sangki Yun, Yi-Chao Chen, and Lili Qiu. 2015. Turning a Mobile Device into a Mouse in the Air. In *Proceedings of the 13th Annual International Conference on Mobile Systems, Applications, and Services*. ACM, Florence Italy, 15–29. <https://doi.org/10.1145/2742647.2742662>
- [84] Sangki Yun, Yi-Chao Chen, and Lili Qiu. 2015. Turning a Mobile Device into a Mouse in the Air. In *Proceedings of the 13th Annual International Conference on Mobile Systems, Applications, and Services*. ACM, Florence Italy, 15–29. <https://dl.acm.org/doi/10.1145/2742647.2742662>
- [85] Sangki Yun, Yi-Chao Chen, Huihuang Zheng, Lili Qiu, and Wenguang Mao. 2017. Strata: Fine-Grained Acoustic-based Device-Free Tracking. In *Proceedings of the 15th Annual International Conference on Mobile Systems, Applications, and Services*. ACM, Niagara Falls New York USA, 15–28. <https://dl.acm.org/doi/10.1145/3081333.3081356>
- [86] Feng Zhang, Chen Chen, Beibei Wang, and K. J. Ray Liu. 2018. WiSpeed: A Statistical Electromagnetic Approach for Device-Free Indoor Speed Estimation. *IEEE Internet of Things Journal* 5, 3 (June 2018), 2163–2177. <https://doi.org/10.1109/JIOT.2018.2826227>
- [87] Yi Zhang, Weiyang Hou, Zheng Yang, and Chenshu Wu. 2023. VECARE: Statistical Acoustic Sensing for Automotive In-Cabin Monitoring. In *USENIX NSDI*.
- [88] Yongzhao Zhang, Hao Pan, Yi-Chao Chen, Lili Qiu, Yu Lu, Guangtao Xue, Jiadi Yu, Feng Lyu, and Haonan Wang. 2023. Addressing Practical Challenges in Acoustic Sensing To Enable Fast Motion Tracking. In *Proceedings of the 22nd International Conference on Information Processing in Sensor Networks*. 82–95.
- [89] Yongzhao Zhang, Yezhou Wang, Lanqing Yang, Mei Wang, Yi-Chao Chen, Lili Qiu, Yihong Liu, Guangtao Xue, and Jiadi Yu. 2023. Acoustic Sensing and Communication Using Metasurface. In *20th USENIX Symposium on Networked Systems Design and Implementation (NSDI 23)*. 1359–1374.
- [90] Yue Zheng, Yi Zhang, Kun Qian, Guidong Zhang, Yunhao Liu, Chenshu Wu, and Zheng Yang. 2019. Zero-effort cross-domain gesture recognition with Wi-Fi. In *Proceedings of the 17th annual international conference on mobile systems, applications, and services*. 313–325.